Parent Ion Resolution in Linked Scans for Dissociations Occurring in the First Field-Free Region of Sector Mass Spectrometers

Kevin D. Ballard and Ralph S. Orkiszewski
Center for Experimental Therapeutics, Baylor College of Medicine, Houston, Texas, USA

Richard W. Vachet and Gary L. Glish
Department of Chemistry, University of North Carolina, Chapel Hill, North Carolina, USA

J. James Vrbanac
Pharmacia & Upjohn, Inc., Drug Metabolism Research, Kalamazoo, Michigan, USA

Simon J. Gaskell
Centre for Mass Spectrometry, UMIST, Manchester, UK

A frequently employed means of studying reactions of ions under high energy collisional activation conditions involves linked scanning a double-focusing mass spectrometer to detect product ions formed in the first field-free region. Experiments have demonstrated that the effective resolution of the parent ion varies during the course of a product ion scan, and this variation is attributed to the kinetic energy released during dissociation. Carefully generated Lacey–Macdonald ion intensity diagrams accurately reflect the dissociation events occurring in various regions of sector mass spectrometers. Consideration of such diagrams leads to an understanding of the noted phenomena and allows the derivation of an expression for the effective parent ion resolution. Furthermore, the approach predicts that parent ion resolution varies during constant neutral loss scans and that the relatively poor resolution (and its variation) can provide particularly misleading data. Results from product ion scans with stable isotope-labeled compounds and constant neutral loss scans with rubidium bromide and stable isotope-labeled peptide derivatives were consistent with the theoretical predictions. (J Am Soc Mass Spectrom 1997, 8, 545–553) © 1997 American Society for Mass Spectrometry

Introduction

The presence of two independent analyzers in a double-focusing mass spectrometer allows tandem mass spectrometry (MS/MS) information to be obtained. The accelerating potential (V) and the fields on the magnetic sector (B) and the electric sector (E) analyzers can be linked together by an appropriate mathematical relationship to provide various types of information about the reactions of ions in the mass spectrometer. Linked scan techniques have been well documented and are widely used to determine fragmentation patterns and ultimately provide structural information for many types of ions [1, 2]. The earliest linked scan method involved varying the electric sector and accelerating potentials at a constant ratio of E^2/V to provide a product ion spectrum [2, 3]. For reactions occurring in the first field-free region (FFR1), a variety of linked scans have been developed to study parent–product ion relationships [4]. The most commonly used linked scans are the product ion scan (with the ratio B/E constant) [5, 6], the parent ion scan (B^2/E held constant) [7], and the neutral loss scan (at constant $[B/E][1 - E/E_0]^{1/2}$) [8, 11].

Although linked scans have been used effectively to provide MS/MS information, the kinetic energy released (T) during the dissociation of an ion affects the resulting spectrum. The effects of T are observed in peak widths (in some scan modes) and in the presence of artifact peaks, which in product ion scans and neutral loss scans may lead to erroneous conclusions about the structure of the ion of interest. Artifact peaks in product ion scans typically arise from the dissociation of parent ions with mass-to-charge (m/z) values close to that of the parent ion "selected." In B/E linked scans, product ions are transmitted to the detector because they have the same velocity as the "selected" parent ion. Due to kinetic energy release, product ions from parent ions of similar m/z to the selected parent

Address reprint requests to Dr. Gary L. Glish, Department of Chemistry, University of North Carolina, CB 3290, Chapel Hill, NC 27599-3290. E-mail: glish@unc.edu

1044-0305/97/$17.00
PII S1044-0305(97)00013-5

Received September 11, 1996
Revised January 15, 1997
Accepted January 16, 1997

ion can gain or lose kinetic energy and be transmitted to the detector because their velocity is similar to that of the selected parent ion. The transmission of undesired product ions gives rise to artifact peaks that are difficult to distinguish from true product ions in the spectrum, although a complicated method has been described to remove these interfering ions [12].

A convenient means of understanding the origin of product ions and artifact peaks is by using Lacey–Macdonald plots [13–15]. This geometric representation uses a two-dimensional coordinate system to describe the instrumental parameters that allow ions to pass through the instrument to the detector. The abscissa (ρ), which is related to the kinetic energies of the ions, is defined as the ratio of the electric sector voltage (E) to pass a given product ion to that of the electric sector voltage (E_0) to pass the parent ion ($\rho = E/E_0$). The ordinate (M^*), which is related to the momenta of the ions, is the conventional mass scale with dissociation products from FFR1 appearing at $M^* = m_d^2/m_p$, in which m_d is the product ion mass and m_p is the parent ion mass. Ion intensities can be plotted in a third dimension. Lacey–Macdonald diagrams provide a means of viewing the various methods of linked scanning and facilitate the understanding of parent–product ion relationships.

The application of Lacey–Macdonald plots allows for a better understanding of the origin of artifact peaks in an MS/MS spectrum. Artifact peaks in product ion scans result when the intensity of one parent ion's dissociation product overlaps the scan line for dissociations of another parent ion. The measured m/z of the product ion being detected is the actual m/z of that product ion; however, that product ion is produced from an ion other than the "selected" parent ion. This can be considered to be a problem in the effective resolution of the parent ion (the term "effective resolution" is used because the parent ion is not physically selected by an analyzer for these experiments). The release of kinetic energy during dissociation along with instrumental operating parameters causes the reduction in the effective parent ion resolution. This article demonstrates that the effective resolution of a parent ion varies during the course of product ion and constant neutral loss scans, and carefully generated Lacey–Macdonald ion intensity diagrams can be used to describe this phenomenon accurately. Also, an equation that includes the masses of the parent ion, product ion, and neutral loss, the kinetic energy release, and the accelerating voltage is derived for the determination of the effective parent ion resolution.

Experimental

Product ion scans and constant neutral loss scans were performed either on a Finnigan MAT900 mass spectrometer (Finnigan MAT, Bremen, Germany; EB geometry) at the University of North Carolina, Chapel Hill, or by using the BE portion of a VG ZAB-SEQ (VG Analytical, Manchester, UK; BEqQ geometry, where q is the rf-only quadrupole and Q is the analyzer quadrupole) at Baylor College of Medicine. In both cases, ions were generated by fast-atom bombardment by using an 8-keV argon or xenon primary atom beam. Product ion scans (B/E) were obtained by simultaneously scanning the magnetic sector and the electric sector field strengths at a constant ratio and were under hardware control. For constant neutral loss scans, the sectors were linked with a relationship of $(B/E)(1 - E/E_0)^{1/2}$; these scans were under hardware control for the MAT900 and under data system control for the ZAB-SEQ.

Tirilazad and its stable isotope-labeled analogs were synthesized by Pharmacia & Upjohn, Inc. (Kalamazoo, MI). Leucine enkephalin (Bachem, Torrance, CA) was labeled at the C-terminus with two ^{18}O atoms through acid catalyzed isotopic exchange with $H_2{}^{18}O$ (Cambridge Isotope Laboratories, Andover, MA) [16]. Unlabeled leucine enkephalin methyl ester was prepared by treating the unlabeled peptide with 3-M HCl/methanol [16]. [$^{18}O_1$]- and [$^{18}O_2$]-leucine enkephalin methyl ester were prepared by treating the [$^{18}O_2$]-labeled peptide with 3-M HCl/methanol and ethereal diazomethane, respectively. [$^2H_3$]-leucine enkephalin methyl ester was similarly prepared using 3-M HCl/[$^2H_3$] methanol (Cambridge). Rubidium bromide was purchased from Aldrich Chemical Company (Milwaukee, WI).

Lacey–Macdonald ion intensity diagrams were generated in the manner described by Boyd and co-workers [17, 18]. Product ion peak half-widths ($w_{1/2}$) due to kinetic energy release were calculated (corrected for the energy spread of the parent ion beam) using a similar approach to that described by Cooks et al. [19]. The elliptical product ion regions in the Lacey–Macdonald diagrams were plotted as plus or minus one half-width (in $w_{1/2}/E_0$ terms).

Results

Product Ion Scan

When a 1:1 mixture of unlabeled tirilazad ($[M + H]^+ = m/z$ 625) and [$^{13}C_3$, $^{15}N_2$]-labeled tirilazad ($[M + H]^+ = m/z$ 630) is used as the sample, and a B/E linked scan for products of the unlabeled parent ion (m/z 625) is performed on the ZAB-SEQ (Figure 1a) and the MAT900 (Figure 1b), the region around m/z 250 consists of peaks at m/z 246 and 251. The peak at m/z 251 is 40% of the intensity of the peak at m/z 246 in the spectrum obtained on the ZAB-SEQ and 75% of the intensity of the peak at m/z 246 in the spectrum obtained on the MAT900. A B/E linked scan of a sample of unlabeled tirilazad alone results in a product ion appearing only at m/z 246 in this same region of the spectrum. Similarly, a B/E linked scan of a sample of [$^{13}C_3$,$^{15}N_2$]-labeled tirilazad results in only a product ion at m/z 251 (that retains all the stable

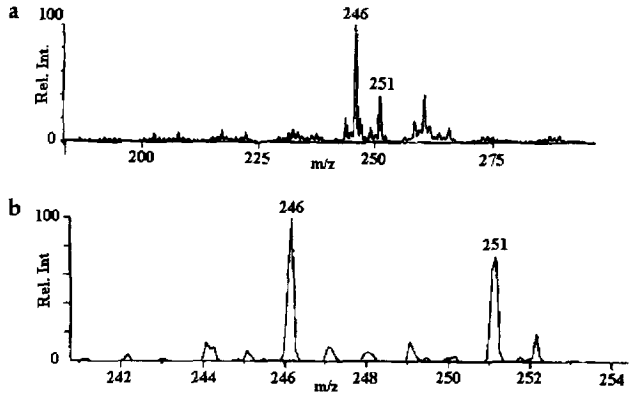

Figure 1. Portion of the B/E linked scan product ion spectrum surrounding the m/z 246 region for unlabeled tirilazad (parent m/z 625) obtained when a 1:1 mixture of unlabeled and [$^{13}C_3$, $^{15}N_2$]-labeled tirilazad was introduced into the ionization source. The spectrum in (**a**) was obtained by using the ZAB-SEQ instrument and the spectrum in (**b**) was obtained using the MAT900.

isotopes) in this region of the spectrum. It is clear from these spectra that an artifact peak at m/z 251 was present when the mixture was used. The unambiguous identification of this peak as m/z 251 was confirmed on the ZAB-SEQ hybrid instrument using the analyzer quadrupole. This peak is due to the dissociation of the labeled tirilazad (m/z 630) parent species; because of the kinetic energy release accompanying the dissociation, a portion of the population of m/z 251 product ions has the same velocity as the "selected" m/z 625 parent. This subpopulation of m/z 251 ions can thus appear as a peak in the B/E linked scanning spectrum for products of the m/z 625 parent ion.

Product ion scans (B/E) of unlabeled tirilazad from a 1:1 mixture of ([$^2H_3$])-labeled ([M + H]$^+$ = m/z 628) and unlabeled tirilazad in different m/z ranges show differing extents of contamination by artifact peaks. In the region around the product ion at m/z 583, an artifact peak at m/z 586 is present at a relative intensity (to m/z 583) of 10% in the spectrum obtained on the ZAB-SEQ and at 55% in the spectrum obtained on the MAT900. In the region around the product ion at m/z 610, an artifact peak at m/z 613 is present in the spectrum obtained on the MAT900 at a relative intensity of 40%. From these results and those in Figure 1, it can be seen that the extent of interference by the artifact peaks is greatest in the lower product ion mass region.

Another component to these phenomena is apparent from comparing the spectra obtained on the two different instruments. In Figure 1 and the other results over different m/z ranges, the relative intensities of the artifact peaks are much greater in the spectra obtained on the MAT900. There are two major differences between the two instruments: (1) the geometry of the sectors (EB vs. BE), and (2) the accelerating potential (V). The variation in sector geometry is not expected to cause any significant differences in artifact intensities because the dissociations in both cases occur in FFR1 and both instruments are scanned with the ratio B/E held constant. It is well established that the order of the sectors is of no significance with B/E linked scanning experiments. The difference in accelerating potential (the MAT900 uses an accelerating voltage of 4750 V, whereas the ZAB uses an accelerating voltage of 8000 V), however, affects the parent ion resolution, as will be discussed further in subsequent text.

Another example of the varying intensity of artifact peaks in different mass windows is evident in the product ion scans of the labeled and unlabeled species of leucine enkephalin methyl ester (Figure 2). Figure 2a shows the product ion scan of [$^{18}O_1$]-labeled leucine enkephalin methyl ester in the presence of equal amounts of the unlabeled and [$^{18}O_2$]-labeled species.

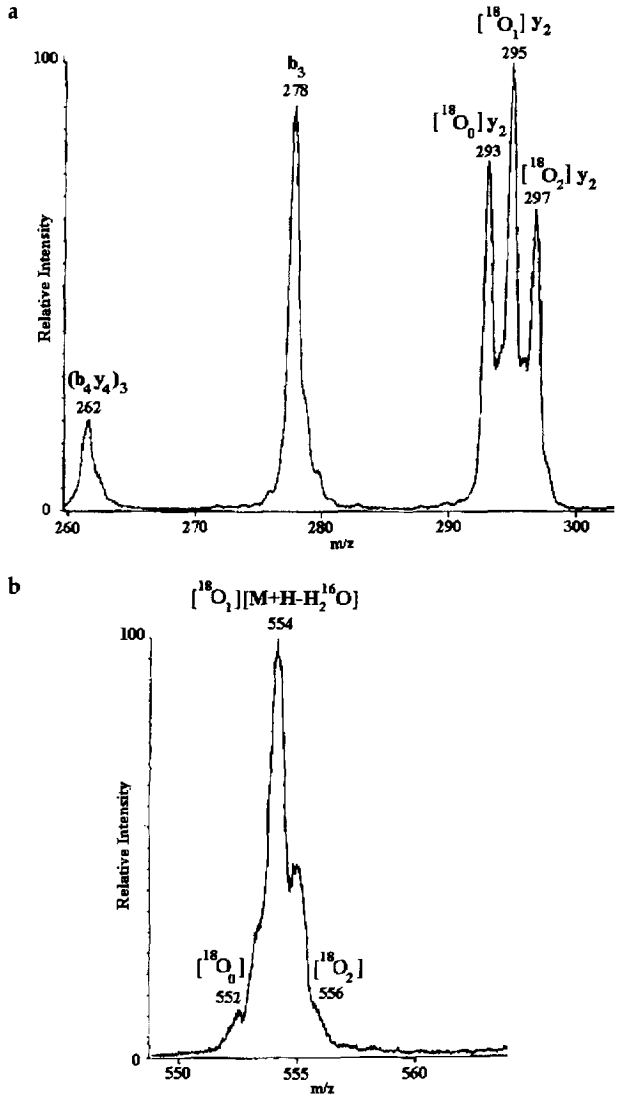

Figure 2. Two regions of the B/E linked scan product ion spectrum, set to detect products of [$^{18}O_1$]-labeled leucine enkephalin methyl ester, obtained with a 1:1:1 mixture of unlabeled, [$^{18}O_1$]-labeled, and [$^{18}O_2$]-labeled species introduced into the source. The spectra were obtained on the ZAB-SEQ instrument.

The spectrum around m/z 295 shows significant interference from product ions derived from both the [$^{18}O_2$]-labeled and the unlabeled leucine enkephalin methyl ester. (The m/z 262 and 278 ions in Figure 2a do not retain the isotopic label, and thus no interfering peaks per se are apparent. However, part of the signal observed for these two ions is due to interference from the naturally occurring ^{13}C isotopic peak of the unlabeled species.) For higher mass product ions (Figure 2b) from the [$^{18}O_1$]-labeled species, the interference by artifact peaks is very slight. (The peak at m/z 555 is due to interference from the naturally occurring ^{13}C isotopic peak of the unlabeled species. Such ^{13}C peaks are in all the spectra.) This follows the trend observed in the case of tirilazad: the higher the ratio of m_d/m_p, the lower the relative intensity of the artifact peaks, and thus the greater the effective parent resolution.

Constant Neutral Loss Scan

Constant neutral loss scans involving isotopomers on two-sector instruments can be especially misleading regarding the effective resolution of the parent ions. This problem arises when isotopomeric parent ions decompose to lose a neutral fragment that retains the isotopic label, i.e., when the parent ions dissociate to yield the same product ion m/z. An example of this phenomenon is shown in Figure 3. Figure 3 shows a region of the constant neutral loss spectrum (neutral loss mass 148) from a 1:1 mixture of unlabeled and [$^2H_3$]-labeled leucine enkephalin methyl ester ([M + H]$^+$ = m/z 570 and 573, respectively). The neutral product chosen for this scan retains the isotopic label, so that both parent ions give rise to m/z 425 product ions (loss of 148 for the labeled ion; loss of 145 for the unlabeled ion). Due to the absence of a significant signal corresponding to the unlabeled parent ion (m/z 570) in Figure 3, it might be tempting to conclude that the parent ions were well resolved by this scan. This is not the case, however, as a corresponding neutral loss scan (neutral loss mass 148) using only the unlabeled species, which ideally should not be detected because its neutral product has a mass of 145, gives a signal at precisely the same location in the spectrum that the mixture did. Thus, the effective parent ion resolution in Figure 3 is actually poor. The intensity of the artifact signal in this neutral loss scan (neutral loss mass 148) of the unlabeled species is lower than the intensity of the "real" peak in the neutral loss scan of the labeled species. A method to predict the artifact peak intensity is the subject of a companion article [20].

These issues can be further illustrated using rubidium bromide. The various possible combinations of natural abundances (^{85}Rb, ^{87}Rb, ^{79}Br, and ^{81}Br) give rise to isotopomeric clusters such as [Rb_3Br_2]$^+$, as illustrated in Figure 4 (theoretical distributions). The loss of the neutral fragment RbBr can correspond to the loss of 163.8, 165.8, or 167.8 from various members of the isotopomeric cluster. None of the isotopomers

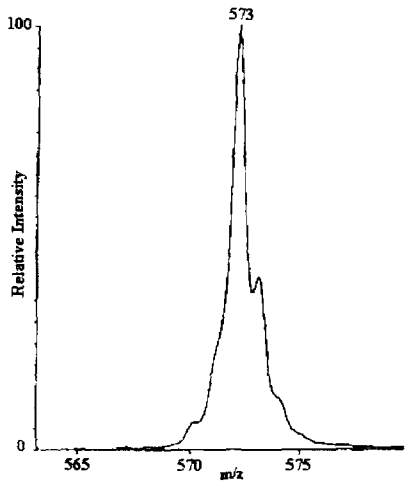

Figure 3. Narrow range of a constant neutral loss scan obtained on the ZAB-SEQ with a 1:1 mixture of unlabeled and [$^2H_3$]-labeled leucine enkephalin methyl ester introduced into the source. The neutral loss mass was 148, corresponding to a fragment retaining three deuterium labels.

can lose 169.8 as a neutral fragment. Nevertheless, when rubidium bromide is analyzed by constant neutral loss scanning with the neutral loss mass set to 169.8, four peaks corresponding to members of the isotopomeric [Rb_3Br_2]$^+$ cluster are detected (Figure 5). This can again be explained through kinetic energy release leading to poor effective parent ion resolution.

Theory and Discussion

Product Ion Scans

It is obvious from the spectra for the product ion scans of tirilazad and leucine enkephalin methyl ester that the artifact peaks that arise from the isotopomers of these two compounds could cause difficulty in the interpretation of the MS/MS spectra. The clearest way to explain this phenomenon is by plotting these dissociations on a Lacey–Macdonald ion intensity diagram. Figure 6 shows a full mass range diagram with the scan functions (B/E = constant) for detecting FFR1 product ions from the unlabeled and [$^{13}C_3{}^{15}N_2$]-labeled species of tirilazad (m/z 625 and 630, respectively). The abscissa ($\rho = E/E_0$) is the ratio of the product ion kinetic energy to that of the parent ion (also equal to m_d/m_p). The ordinate (M^*) is the apparent mass of the product ion in the conventional mass spectrum. FFR1 dissociation product ions appear at $M^* = m_d^2/m_p$ in a conventional mass spectrum (i.e., on an instrument with no electric sector). On such diagrams, dissociation reactions are shown as elliptical ion intensity regions (the ellipses are very small on the scan line and are not noticeable on this plot, which is drawn to scale).

The bottom inset in Figure 6 is an expanded view of the region indicated. The ellipses representing the dissociations are centered at the (E/E_0, M^*) values

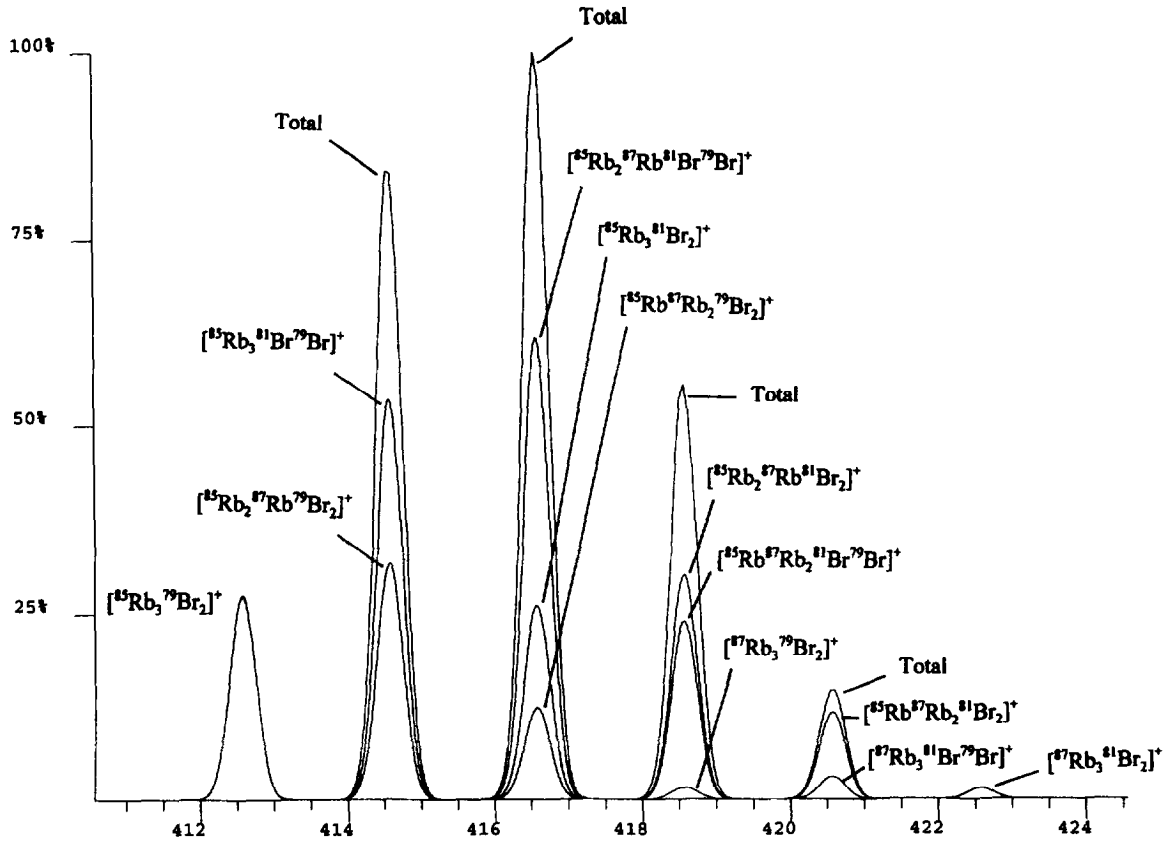

Figure 4. The various possible combinations and natural abundances of isotopomers of rubidium and bromide (^{85}Rb, ^{87}Rb, ^{79}Br, and ^{81}Br) that give rise to the isotopomeric clusters of $[Rb_3Br_2]^+$. The multiple peaks at individual masses indicate the natural abundances of the isotopomers that constitute that particular mass.

appropriate for the dissociation. The corresponding constant B/E linked scan for the FFR1 dissociation necessarily passes through the center of each ellipse. The length of the major axis of the ellipse is calculated from the kinetic energy release and the instrument's energy resolving power (subsequently detailed), and

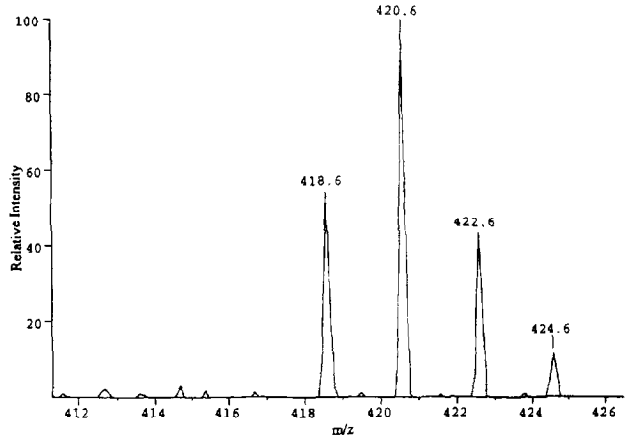

Figure 5. Constant neutral loss spectrum of rubidium bromide obtained on the MAT900, with the instrument set to detect the impossible loss of a neutral fragment of 169.8 Da.

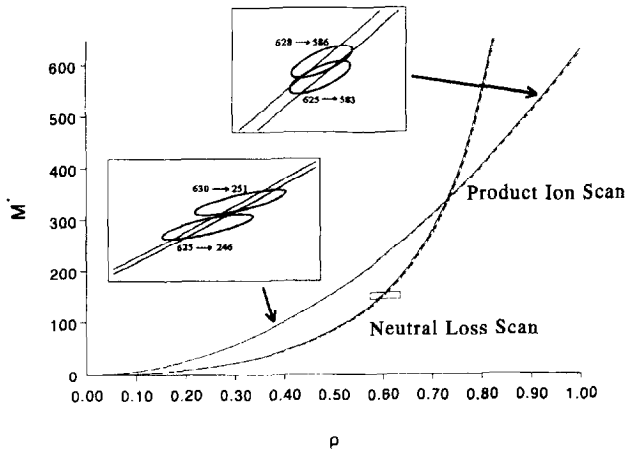

Figure 6. Full range Lacey–Macdonald ion intensity diagram depicting the complete product ion scan functions (B/E) for unlabeled (m/z 625) and [$^{13}C_3$, $^{15}N_2$]-labeled tirilazad (m/z 630) and the complete scan functions for the constant neutral losses involving the fragment masses of 163.8, 165.8, 167.8, and the impossible neutral loss of 169.8 from rubidium bromide clusters. The bottom inset depicts an expanded view of the indicated region corresponding to the dissociations of m/z 625 to 246 and m/z 630 to 251. The top inset shows an expanded view of the indicated region for the dissociations of m/z 625 to 583 and m/z 628 to 586.

the ellipse represents all ionic species within plus or minus one half-width (in E/E_0 terms). The vertical (minor) axis of the ellipse is determined by the instrument's ability to resolve the detected product ions: the magnitude of the minor axis is relatively unimportant for these considerations because it does not contribute significantly to the spread in the resolution. Ion intensity is actually the third dimension of these plots, and the ellipse represents a horizontal cross section (taken at half-height) through the three-dimensional ion intensity region.

The bottom inset in Figure 6 shows ellipses representing the two decompositions of m/z 625 to 246 and m/z 630 to 251. The length of the major axis of each ellipse is calculated in the following manner. Starting with the equations for the kinetic energy release (eq 1) and the correction for the energy spread inherent in the parent ion beam (eq 2), substituting ΔE and solving for the half-width in terms of the ρ scale (E/E_0) gives eq 3:

$$T = \left(\frac{m_p^2 eV}{16 m_d m_n}\right)\left(\frac{\Delta E}{E_0}\right)^2 \quad (1)$$

$$\Delta E = \sqrt{(w_{1/2})^2 - (w_m)^2} \quad (2)$$

$$\frac{w_{1/2}}{E_0} = \sqrt{\frac{16 T m_d m_n}{m_p^2 eV} + \left(\frac{w_m}{E_0}\right)^2} \quad (3)$$

where m_p, m_d, and m_n are the masses of the parent ion, product ion, and neutral loss, respectively. ΔE is the corrected peak width at half-height on an energy scale (from an electric sector scan or a parent ion linked scan) for the dissociation with $w_{1/2}$ and w_m as the peak widths for the peak measured in the spectrum and the parent ion beam, respectively. V is the accelerating voltage and E_0 is the kinetic energy of the parent ion beam. The value obtained from eq 3 gives the length of the major axis extended in each direction from the center of the ellipse. The center of the ellipse is determined from $\rho = m_d/m_p$ and $M^* = m_d^2/m_p = \rho m_d$. The left endpoint of the major axis (ρ_l', $M_l^{*\prime}$) is determined by eqs 4 and 5.

$$\rho_l' = \rho - \frac{w_{1/2}}{E_0} \quad (4)$$

$$M_l^{*\prime} = (\rho_l')(m_d) \quad (5)$$

The right endpoint (ρ_r', $M_r^{*\prime}$) is determined by eqs 6 and 7:

$$\rho_r' = \rho + \frac{w_{1/2}}{E_0} \quad (6)$$

$$M_r^{*\prime} = (\rho_r')(m_d) \quad (7)$$

The minor axis of the ellipse is determined by the instrument's product ion resolution. Under the conditions employed for these experiments, the MAT900 has a product ion resolution of 1000 and the ZAB has a product ion resolution of about 500. The extent of the minor axis can be calculated for the ZAB in terms of M^* by

$$\text{min} = \frac{(m_d + m_d/500)^2}{m_p} - \frac{(m_d)^2}{m_p} \quad (8)$$

Equation 8 gives the coordinates of the minor axis as (ρ, M^* + min) and (ρ, M^* − min).

By using 8 kV for the accelerating potential (V), 0.001 for the energy resolution (w_m/E_0) of the instrument, and 0.09 eV as the measured kinetic energy release for these dissociations, the ellipses for these product ion formations can be plotted (bottom inset, Figure 6). [The value for the kinetic energy release (T) was obtained from a separate experiment (E scan or B^2/E scan). The corrected width of a peak at half-height (ΔE) in energy units corresponding to the dissociation of interest was inserted into eq 1, and the T was calculated with the other variables known.] From this plot, it is clear why an artifact peak appears in the B/E linked scan for products of m/z 625 (unlabeled tirilazad) from a 1:1 mixture of unlabeled and [$^{13}C_3{}^{15}N_2$]-labeled tirilazad. The ellipse created by the m/z 630 to 251 dissociation is intersected by the m/z 625 scan line to some extent, resulting in m/z 251 appearing in the MS/MS spectrum of m/z 625. Ellipses for these dissociations, using the MAT900 parameters (not shown) are larger due to the lower energy resolution and lower accelerating voltage. The larger ellipses result in a greater degree of scan line intersection, and therefore more intense artifact peaks.

The presence of an artifact peak with a smaller relative intensity in the region around the product ion m/z 583 from the unlabeled species of tirilazad can be understood by viewing the ellipses generated by this dissociation (top inset, Figure 6). Even though the ellipses overlap each other significantly, the ellipse from the dissociation of m/z 628 to 586 is intersected by the scan line for m/z 625 to a lesser extent than in the previous example. This is due almost entirely to the scan lines of the labeled and unlabeled species being more separated at higher m_d/m_p ratio (even though this example involves parent ions differing in mass by only 3 Da, whereas in the previous example the masses differed by 5 Da). This difference in distance between scan lines as a function of the m_d/m_p ratio leads to the variance in the effective resolution of the parent ion. At smaller ratios of m_d/m_p the scan lines are closer on the Lacey–Macdonald diagrams; thus, the ellipses intersect adjacent scan lines to greater extents and artifact peaks are seen at greater intensities.

Neutral Loss Scans

The results from the constant neutral loss scans can be similarly understood by employing Lacey–Macdonald ion intensity diagrams. Figure 6 also shows the full range ion intensity diagram for the constant neutral loss scans of 163.8, 165.8, 167.8, and 169.8. Figure 7 shows an expanded view of the rectangular region indicated in Figure 6 for the four possible dissociations of the isotopomers of $[Rb_3Br_2]^+$ involving a neutral loss of 167.8 (solid ellipses) and the four possible dissociations of the isotopomers of $[Rb_3Br_2]^+$ involving the neutral loss of 165.8 (dashed ellipses). The ellipses were calculated in the same manner as described in the foregoing text. The scan line for the impossible neutral loss of 169.8 passes through and crosses the major axis of each of the eight ion intensity regions in Figure 7 (in fact, the four pairs of ellipses overlap a continuum of neutral loss scan lines up to a constant neutral loss of about 172). Dissociations involving a neutral loss of 163.8 do not overlap the scan line of 169.8 and therefore need not be considered here. The dissociations shown in Figure 7 comprise four pairs of overlapping, coaxial ellipses, with each member of a pair giving rise to product ions of the same nominal mass. The four pairs of fragmentations thus give rise to four nominal product ions of m/z 254.8, 252.8, 250.8, and 248.8. Thus, the four peaks observed in Figure 5 were due to the four pairs of dissociations involving these four product ions. Since the scan accurately measures the product ion's m/z, the apparent masses of the parent ions observed in Figure 5 are simply the masses of the detected product ions plus the neutral loss mass for the scan function. Note that neutral loss scans of, for example, 170 or 171.5 (or anything up to 172) would also give a result similar to that obtained in the neutral loss scan of 169.8.

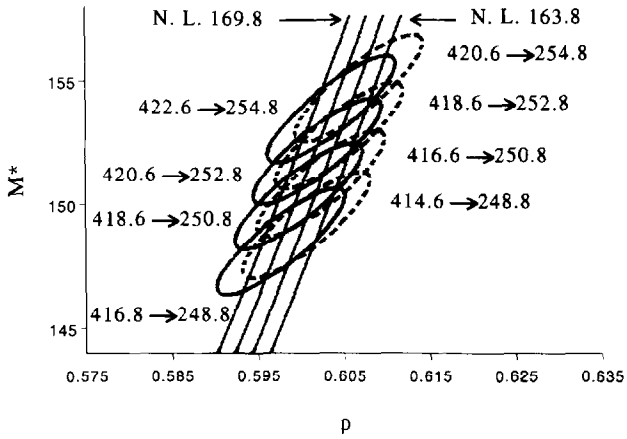

Figure 7. Expanded Lacey–Macdonald ion intensity diagram depicting the four possible dissociations of the isotopomers of $[Rb_3Br_2]^+$ involving a neutral loss of 167.8 (solid ellipses) and the four possible dissociations involving a neutral loss of 165.8 (dashed ellipses). The scan functions shown represent constant neutral loss scans involving isotopomeric fragment masses of 163.8, 165.8, and 167.8, and the impossible neutral loss of 169.8 Da.

Parent and Neutral Loss Resolution

To generalize this discussion and provide a relationship that would describe the effective parent ion resolution in a B/E linked scan, a hypothetical plot of the dissociation reaction of m/z 1000 to 500 has been constructed (Figure 8). This example assumes that the kinetic energy release is 0.1 eV, the instrument uses an accelerating voltage of 8000 V, and has an energy resolution of 0.001 eV. The approach uses the methods described previously for generating the ellipse. If it is considered that the left endpoint of the major axis of this ellipse defines the center point for a new ellipse, then the center of the new ellipse defines a new B/E linked scan function incorporating the dissociation ($m_{pl} \rightarrow m/z$ 500). The new parent ion scan line is just resolved from the ellipse created by the dissociation of m/z 1000 to 500. Equation 9 can be used to calculate m_{pl}:

$$m_{pl} = \frac{M_1^{*\prime}}{(\rho_1')^2} \tag{9}$$

This calculation gives a value of 1015.4, and therefore the effective parent ion resolution (R) is determined by eq 10 to be 65:

$$R = \frac{m_p}{\Delta m_p} \tag{10}$$

From this hypothetical situation a generic expression can be derived that describes the effective parent ion resolution (R) as a function of m_p, m_d, m_n, T, w_m/E_0, and V. By using eqs 1–9 to determine m_{pl} and comparing it to m_p by eq 10, an expression for the

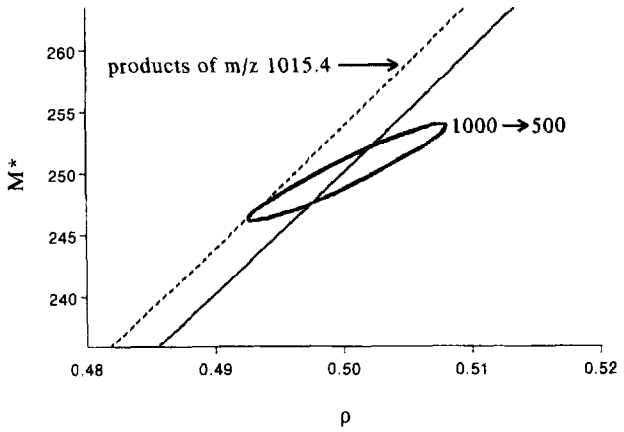

Figure 8. Expanded Lacey–Macdonald ion intensity diagram for the hypothetical fragmentation of an m/z 1000 parent ion to an m/z 500 product ion. The solid curve is the scan function for products of m/z 1000. The dashed curve is the scan function for products of the calculated parent ion (m/z 1015.4), which can be considered just resolved from the m/z 1000 to 500 fragmentation (see text).

effective parent ion resolution (R) can be produced:

$$R = m_p \Bigg/ \left(m_p - \left(m_d \Bigg/ \left(\frac{m_d}{m_p} \pm \sqrt{\frac{16Tm_d m_n}{m_p^2 eV} + \left(\frac{w_m}{E_0}\right)^2} \right) \right) \right) \quad (11)$$

Deriving an equation for the parent ion resolution for constant neutral loss scans results in the same expression as eq 11. However, if a neutral loss resolution (R_{nl}) is considered (i.e., the selection of a neutral loss whose scan line is no longer intersected by the ellipse of another dissociation), a different expression can be derived:

$$R_{nl} = m_n \Bigg/ \left(m_n - \left(m_d \Bigg/ \left(\frac{m_d}{m_p} \pm \sqrt{\frac{16Tm_d m_n}{m_p^2 eV} + \left(\frac{w_m}{E_0}\right)^2} \right) \right) + m_d \right) \quad (12)$$

To illustrate eq 11 and its bearing upon the experimental results, the parent resolution (eq 11) was plotted against various parameters to reveal their relationships (Figure 9) Figure 9a shows a plot of the effective parent ion resolution versus the ratio of the product ion mass to the parent ion mass (m_d/m_p) for kinetic energy releases of 0.1, 0.01, and 0.001 eV. It is clear from this graph that the parent ion resolution varies throughout the scan, as was observed experimentally. At very low product ion mass to parent ion mass ratios, the parent ion resolution is very poor and thus B/E linked scans show significant artifact peaks at low m_d/m_p ratios. At higher m_d/m_p ratios, the resolution is much better. Another obvious trend from Figure 9a is that higher kinetic energy releases lead to lower parent ion resolution. This decrease can be understood by considering that the major axis of the ion intensity ellipse in the Lacey–Macdonald plot expands as a result of the higher kinetic energy release. This expansion causes the ion intensity ellipse to overlap the adjacent scan line to a greater extent and thus reduce the effective parent ion resolution. Typical values of T for collision-induced dissociation are in the 0.05–0.15-

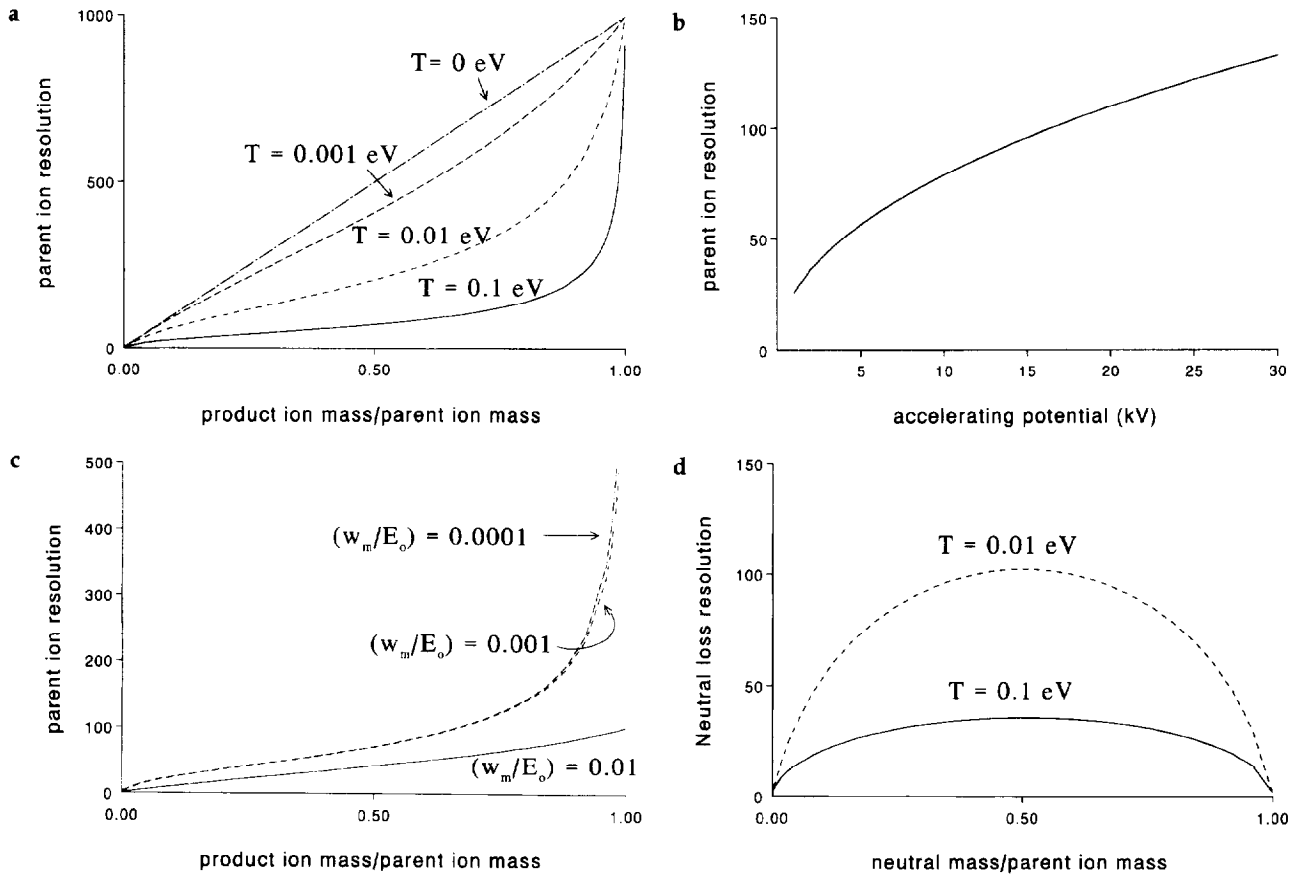

Figure 9. (**a**) Plot of the effective parent ion resolution during a product ion scan versus the ratio of the product ion mass to the parent ion mass (m_d/m_p) for kinetic energy releases of 0.1, 0.01, 0.001, and 0 eV (V = 8000, w_m/E_0 = 0.001). (**b**) Plot of the effective parent ion resolution during a product ion scan versus accelerating voltage (T = 0.1 eV, m_p = 1000, m_d = 500, m_n = 500, w_m/E_0 = 0.001). (**c**) Plot of the effective parent ion resolution during a product ion scan versus m_d/m_p at different energy resolutions (w_m/E_0) (T = 0.1 eV, V = 8000). (**d**) Plot of neutral loss resolution (eq 13) during a constant neutral loss scan versus the ratio of the neutral loss mass to the parent ion mass (m_n/m_p) at different values of kinetic energy release (T) (V = 8000, w_m/E_0 = 0.001).

eV range. Therefore, for most of the scan range, the parent resolution is less than 200.

Figure 9b shows a plot of parent ion resolution versus accelerating voltage. From this plot it is apparent that lower effective parent ion resolution is obtained at lower accelerating voltages. This follows well with the experimental data gathered on the two different instruments. The MAT900, which uses a lower accelerating potential, provides lower parent ion resolution and therefore more interference due to artifact peaks. A plot of parent ion resolution with respect to m_d/m_p at different energy resolutions (w_m/E_0) shows that substantial increases in energy resolution do not drastically affect the parent ion resolution (Figure 9c).

A plot of neutral loss resolution (eq 12) versus the ratio of the neutral loss mass to the parent ion mass (m_n/m_p) at different values of T is revealing about the variation of neutral loss resolution (Figure 9d). The neutral loss resolution is greatest when m_n/m_p has a value of 0.5 and lowest at high and low ratios. For typical kinetic energy releases the neutral loss resolution is less than 50.

Conclusions

During product ion and constant neutral loss scanning experiments involving FFRI dissociations on two-sector instruments, the effective resolution of the parent ion varies during the course of the scan due to the effects of kinetic energy release and as a function of instrumental parameters (accelerating voltage and energy resolution). In the absence of kinetic energy release, the effective parent ion resolution increases linearly with the increasing product ion mass to parent ion mass ratio (m_d/m_p). Using Lacey–Macdonald ion intensity diagrams illustrates the influence of kinetic energy release on parent resolution and the nature of the resulting variations. A theoretical treatment based on Lacey–Macdonald plots has led to an expression that defines the relationship between the parent ion resolution and various parameters. Constant neutral loss scans on two-sector instruments can be especially deceptive regarding the effective resolution of the parent ions because signals due to interfering parent–product relationships can precisely overlap with the intended signal. The effective parent ion resolution is particularly low in dissociations that occur with large releases of kinetic energy. Moreover, the occurrence of sequential fragmentations can cause further kinetic energy spread in the product ions, further reducing the effective parent resolution for a particular product ion. Thus, the parent resolution at a given point during the scan can deviate substantially from the general trend due to variations in kinetic energy release for the individual dissociation reactions. Parent ion resolution is increased by using higher accelerating potentials, but increasing energy-resolving power (w_m/E_0) gives little increase in parent ion resolution over most of the scan range. Therefore, opening up the slits and maximizing signal does not predispose the experiment to significantly increased interference from artifact peaks.

Acknowledgment

The authors are grateful to Dr. Robert K. Boyd for useful discussions during the course of these studies.

References

1. Boyd, R. K. *Mass Spectrom. Rev.* **1994**, *13*, 359.
2. Lacey, M. J.; Macdonald, C. G. *J. Chem. Soc. Chem. Commun.* **1975**, 421.
3. Weston, A. F.; Jennings, K. R.; Evans, S.; Elliott, R. M. *Int. J. Mass Spectrom. Ion Phys.* **1976**, *20*, 317.
4. Busch, K. L.; Glish, G. L.; McLuckey, S. A. *Mass Spectrometry / Mass Spectrometry: Techniques and Applications of Tandem Mass Spectrometry*; VCH: New York, 1988.
5. Millington, D. S.; Smith, J. A. *Org. Mass Spectrom.* **1977**, *12*, 264.
6. Bruins, A. P.; Jennings, K. R.; Evans, S. *Int. J. Mass Spectrom. Ion Phys.* **1978**, *26*, 395.
7. Evers, E. A. I. M.; Noest, A. J.; Akkerman, O. S. *Org. Mass Spectrom.* **1977**, *12*, 419.
8. Zakett, D.; Schoen, A. E.; Kondrat, R. W.; Cooks, R. G. *J. Am. Chem. Soc.* **1979**, *101*, 6781.
9. Haddon, W. F., *Org. Mass Spectrom.* **1980**, *15*, 539.
10. Boyd, R. K.; Porter, C. J.; Benyon, J. H. *Int. J. Mass Spectrom. Ion Phys.* **1982**, *44*, 199.
11. Shushan, B.; Boyd, R. K. *Anal. Chem.* **1981**, *53*, 421.
12. Shushan, B.; Boyd, R. K. *Int. J. Mass Spectrom. Ion Phys.* **1980**, *34*, 37.
13. Lacey, M. J.; Macdonald, C. G. *Org. Mass Spectrom.* **1977**, *12*, 587.
14. Lacey, M. J.; Macdonald, C. G. *Org. Mass Spectrom.* **1978**, *13*, 243.
15. Lacey, M. J.; Macdonald, C. G. *Org. Mass Spectrom.* **1978**, *13*, 284.
16. Thorne, G. C.; Ballard, K. D.; Gaskell, S. J. *Am. Soc. Mass Spectrom.* **1990**, *1*, 249.
17. Boyd, R. K. *Int. J. Mass Spectrom. Ion Processes* **1987**, *75*, 243.
18. Alexander, A. J.; Thibault, P.; Guevremont, R.; Boyd, R. K. *Rapid Commun. Mass Spectrom.* **1988**, *2*, 79.
19. Cooks, R. G.; Benyon, J. H.; Caprioli, R. M.; Lester, G. R. *Metastable Ions*; Elsevier: New York, 1973.
20. Vachet, R. W.; Glish, G. L.; Ballard, K. D.; Orkiszewski, R. S. *J. Am. Soc. Mass Spectrom.* **1997**, *8*, 554–560.